Noname manuscript No.
(will be inserted by the editor)

Memristive PAD three-dimensional emotion generation system based on D-S evidence theory

Mengxian Zhang · Chunhua Wang · Yichuang Sun · Tao Li

Received: date / Accepted: date

Abstract In this work, a Pleasure-Arousal-Dominance (PAD) three-dimensional brain-like emotion generation system is proposed by simulating the brain tissue structures involved in emotion generation in the brain's limbic system. The system utilizes volatile memristors to simulate the activation and recovery process of neurons, and non-volatile memristors to simulate the synaptic weight changes. It combines the brain emotion learning (BEL) model and the biological long short-term memory (B-LSTM) model to simulate the emotion generation process in the brain. The system employs the Dempster-Shafter (D-S) evidence theory for multimodal feature fusion, ultimately representing the generated human-like emotions in the PAD three-dimensional emotion expression space. Considering the differences in emotional information represented in each dimension of the PAD emotion expression space, this work proposes the use of the D-S evidence theory to calculate the weight values of multimodal evidence and each dimension of emotion signals. The system performs weighted summation for multimodal feature fusion, which is more biologically-inspired and realistic. As a result, the generated emotion signals are more accurate, and the PAD three-dimensional emotion expression model enhances the capability and richness of emotion expression. The system processes multimodal input signals (text, speech, visual signals) to generate three-dimensional emotion signals (pleasure, arousal, and dominance signals), which correspond to specific emotions in a three-dimensional space. These signals can be visually represented as facial images using MATLAB. The simulation results from PSPICE indicate a non-linear mapping relationship between the system's input and output. It shows that different inputs can generate distinct human-like emotions.

Keywords PAD model · D-S evidence theory · Memristor · Emotion generation

M. Zhang · C. Wang ✉ · T. Li
College of Computer Science and Electronic Engineering, Hunan University, Changsha, 410082, People's Republic of China
E-mail: wch1227164@hnu.edu.cn

Y. Sun
School of Engineering and Computer Science, University of Hertfordshire, Hatfield, AL10 9AB, United Kingdom.

1 Introduction

With the development of artificial intelligence, it has been comparable to or even more than human beings in computational intelligence and perceptual intelligence, but there is still a certain gap with human beings in cognitive intelligence. To realize artificial intelligence at the human level, it is necessary to learn from the brain's learning and memory functions and give computer human wisdom. Brain-like intelligence [1, 2] research has become a hot spot. Emotion, as an advanced function of the brain, not only ensures the survival and adaptation of organisms, but also affects individual learning, memory and decision-making. The generation and influence of emotion in the brain are closely related to the limbic system [3, 4]. The limbic system is a functional anatomical system composed of the structures of the limbic lobe of the brain (parahippocampus, cingulate gyrus, dentate gyrus, subcallosal gyrus) and subcortical regions (hippocampus, amygdala, habenula, anterior thalamic nucleus, mammillary body) [5]. It is involved in learning and memory activities and affects and produces emotions [6]. By learning the emotional generation mechanism of the brain and study-

ing related models or algorithms, machines can be endowed with human emotions and linked to perception, cognition, motivation and action. In 2001, Morén and Balkenius [7] proposed a brain emotion learning model (BEL), which gives a neurally inspired computational model of the amygdala and the orbitofrontal cortex. The learning process is achieved by continuously adjusting the weights of the amygdala and the orbitofrontal cortex, aiming to partially replicate the same characteristics as the biological system. The BEL model has been applied to automatic control problems [8, 9] and improved classification problems [10,11]. In order to improve the generality of the BEL model, Lotfi *et al.* [12] proposed brain emotional learning-based pattern recognizer to solve the multiple input-multiple output classification and chaotic time series prediction problems. To improve the performance of the BEL model, Ying *et al.* [13] proposed an brain emotional learning model combined with self-adaptive genetic algorithm (AGA) for chaotic prediction and used AGA for parameter optimization, which improved the prediction accuracy and execution speed. The construction of the emotional learning model is very important for the study of brain-like bionic emotions. Multimodal information can learn and generate emotions by feature fusion through the constructed emotional learning loop.

In the field of software, people primarily achieve human-like emotion generation through designing frameworks and utilizing neural network [14–18] algorithms, among other methods. Chae *et al.* [19] propose a methodology for producing robotic emotions suitable for a robot's utterances based on texts. Using the A-star algorithm to generate the path of emotional change, the robot can generate human-like emotional change patterns and recover its emotional state. Li *et al.* [20] propose a method for expressing reactive emotion by dividing the system's emotion into emotion categories and emotion levels, Combining emotional categories, emotional levels, and reverse channels with corresponding emotional categories to set emotional generation rules to generate reactive emotions. Churamani *et al.* [21] propose a novel framework for affect-driven behaviour generation in social robots. The recurrent self-organising neural networks are used to model the affective core of the robot and modulate the robot's affective appraisal. Hong *et al.* [22] proposed a novel multimodal emotional HRI architecture, which determines its emotional behavior via an innovative two-layer emotional model consisting of deliberative (hidden Markov model) and reactive (rule-based) layers. However, compared with the hardware circuit to achieve the brain-like emotion generation system, the running speed of the system realized by software is slower.

In terms of hardware, the traditional von Neumann computing system involves separate processing and storage units. The frequent access operation of data between storage and processing units brings problems such as high power consumption and high delay [23]. As an emerging memory device, the memristor can improve information processing efficiency and reduce power consumption by using its in-situ computing characteristics [24]. In addition, the performance of memristors is similar to that of biological neurons and synapses [25], which can reduce the area and complexity of neuromorphic circuits and is very suitable for constructing brain-like bionic systems. Memristor-based applications are very extensive, such as memory [26, 27], memristive neural networks [28–35], and memristive chaotic circuits [36–41]. Based on the characteristics of memristor, the application of bionic emotion generation is gradually increasing. For example, Ma *et al.* [42] designed a neural network architecture based on memristors to simulate human emotions. They considered the excitation and inhibition between different neurons, achieving a simple simulation of human emotions such as happiness and sadness. Wang *et al.* [43] designed an emotion generation circuit based on memristor to simulate the human skin sensor according to the sensory mechanism of human skin, complex emotions consist of four basic emotions: happiness, anger, sadness and fear. Sun *et al.* [44] developed a memristive circuit based on a second-order damping system to generate certain emotions under different personality traits. They expressed the emotions of anger, sorrow, happiness, and joy through human gestures. However, they did not draw inspiration from the emotional learning and generation process in the brain, lacking neural and biomimetic characteristics. Zhou *et al.* [45] proposed a bionic dual-loop emotional learning circuit that simulates emotional learning in the human brain. This circuit generated four types of emotions: extremely happy, happy, sad, and particularly sad. However, with further development of memristive brain-like emotion generation, it was found that most of their models used discrete emotion models [46], [47] in emotional expression. The discrete emotional model uses adjective labels to represent emotions as several relatively independent sentiment categories. The advantage is simple and easy to analyze. The disadvantage is that the types of emotional states described are limited, and the process of emotional change cannot be intuitively reflected, resulting in the dimensional emotional model. Zhang *et al.* [48] drew inspiration from psychology's theory of emotion generation through reward and punishment. They proposed an operant conditioning model and memristive circuit implementation based on emo-

tion generation and modulation. Using the rolls emotion model, they expressed one-dimensional emotions under four conditions: reward onset, reward termination, punishment onset, and punishment termination. Wang *et al*. [49] combines the memristor with the brain emotion generation mechanism in the limbic system to express emotions in two-dimensional space. Similarly, Wang *et al*. [50] considered the internal regulation and external stimulation factors, which can realize the brain's conscious and unconscious emotional learning and generation process. In [49], [50], the Valence-Arousal (V-A) dimension emotion model [51] is used to describe the emotional state as a certain coordinate in the two-dimensional space with the valence dimension and the arousal dimension. It can track the development and change process of emotion and measure the similarity and differences of emotion, and the emotional expression range is richer than the discrete emotion model. However, the V-A model has a limited range in expressing emotions and cannot fully capture the breadth of human emotions. The designed emotion generation circuit does not adequately consider the dimensional differences in emotions. The weight values between multimodal input signals and each dimension of emotion signal are influenced by the emotional dimension. Therefore, it is necessary to consider multimodal feature fusion methods to obtain more accurate emotional signal results. To address these issues, we propose a memristive Pleasure-Arousal-Dominance(PAD) three-dimensional emotion generation system based on the D-S evidence theory. The main contributions of our system are as follows:

1. A PAD three-dimensional emotion generation system is proposed that uses the pleasure dimension, arousal dimension, and dominance dimension to represent human-like emotions. The PAD emotion model effectively explains human emotions, making the emotional expression of the system more comprehensive and accurate.
2. Taking into account the differences in information for each dimension of emotion, we propose the use of the D-S evidence theory to calculate the weight values between multimodal evidence and each dimension of emotion signal. The system performs multimodal feature fusion through weighted summation, which is more biomimetic and realistic, resulting in more accurate emotional signal results.
3. Leveraging the in-situ computing characteristics of memristors, we construct synapses and neurons and combine the BEL model and B-LSTM model to build the brain's cortical structure of the limbic system of the brain. This optimization of the circuit structure is achieved.

The rest of this article is organized as follows. Section 2 introduces the proposed PAD three-dimensional emotion generation system. Section 3 introduces the volatile and non-volatile memristor models for constructing synaptic and neuronal modules. Section 4 introduces the specific circuit design. By simulating the hypothalamus, sensory cortex, orbital frontal cortex and amygdala module, the brain emotion generation circuit is constructed to obtain three-dimensional emotional signals. Section 5 shows the simulation results of the proposed circuit and analyzes them to verify the feasibility of the the designed PAD three-dimensional emotion generation memristive circuit. Section 6 presents the conclusions drawn from this work and discusses further work.

2 PAD three-dimensional emotion generation system

2.1 PAD emotion expression model

Commonly used dimensional emotional expression models include the V-A model [51] and the PAD model [52]. The V-A model [51] is the 'Valence-Arousal' model, and the PAD emotion model [52] is the 'Pleasure-Arousal-Dominance' model. The pleasure dimension, also known as the valence dimension, is a measure of the degree of pleasure of a person, from one extreme (distress) to another extreme (ecstasy); the arousal dimension, also known as the activation dimension, is a measure of physiological activity and psychological alertness. For example, sleep and boredom are low arousal, and waking and tension are high arousal; the dominance dimension is also called the Attention dimension or the Power dimension. It refers to the subject's control of the situation and others. High dominance is a powerful and dominant sense, while low dominance is a sense of withdrawal and weakness.

This work uses the PAD three-dimensional emotion model to represent emotions, and each dimension is a measure of a certain aspect of emotion. The V-A model can express most of the emotions, while the PAD model can theoretically represent an infinite variety of emotions. the PAD model increases the dominance dimension compared with the V-A model, has a stronger ability to express the emotions, and can effectively explain human emotions, then the system's expression of emotions is more comprehensive and accurate. The two emotional expression models are shown in Fig. 1.

As shown in Fig.1, fear and anger are both emotions characterized by low pleasure and high arousal, located in the second quadrant of the V-A two-dimensional space. This makes it difficult to distinguish between

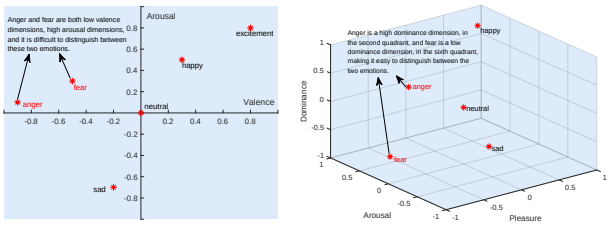

(a) (b)

Fig. 1 Emotional expression models. (a) is a V-A two-dimensional emotional expression model, including the valence dimension and arousal dimension. (b) is a PAD three-dimensional emotional expression model, including pleasure dimension, arousal dimension and dominance dimension, with stronger emotional expression ability and richer emotional expression range.

these two emotions. However, in the PAD three-dimensional space, fear is characterized by low dominance and is located in the sixth quadrant, while anger is characterized by high dominance and is located in the second quadrant. This allows for a better differentiation between these two emotions. Therefore, using the PAD three-dimensional emotion model can provide a more comprehensive and accurate representation of emotions.

2.2 D-S evidence theory

D-S evidence theory [53] was originally proposed by Dempster and improved by Shafter. It uses the D-S synthesis rule to fuse the trust functions from different evidence bodies into a new trust function to obtain more reliable decision results. Under the assumption that the recognition framework $\theta = \{c_1, c_2, ..., c_c\}$ represents the set of results that can be identified by the decision problem, a set function $m : 2^{\Theta} \rightarrow [0, 1]$ is defined as the basic probability assignment function (BPA) on Θ and satisfies:

$$\begin{cases} m(\phi) = 0 \\ \sum\limits_{A \subseteq \Theta} m(A) = 1 \end{cases} \tag{1}$$

where ϕ denotes the empty set, and $m(A)$ denotes the confidence of the evidence to A. Let m_1, m_2 be the basic probability assignment function of different evidences on Θ, then according to the combination rule of D-S evidence theory, the fused basic probability assignment function $m = m_1 \oplus m_2$ is :

$$\begin{cases} m(\phi) = 0 \\ m(c) = \sum\limits_{A_i \cap B_j = \phi} \frac{m_1(A_i) m_2(B_j)}{1-K}, c \neq \phi \end{cases} \tag{2}$$

where $K = \sum\limits_{A_i \cap B_j = \phi} m_1(A_i) m_2(B_j)$ is a conflict factor, reflecting the degree of conflict between evidences. The greater the value, the greater the conflict between evidences.

The multimodal input signals include text signals, speech signals, and visual signals. This work uses the D-S theory to calculate the probability distribution function after evidence fusion to obtain the weight distribution results between the multimodal signals and each dimension of the emotional signals. Each dimension in the PAD three-dimensional emotion model is a measure of a certain aspect of the emotion, including pleasure, arousal, and dominance. Therefore, this work uses the D-S evidence theory three times to obtain weight allocation results influenced by emotional signals. The use of D-S evidence theory allows the system to more accurately characterize the emotional differences of each dimension.

2.3 Flowchart of the PAD three-dimensional emotion generation system

In this work, a PAD three-dimensional emotion generation system is proposed. The PAD three-dimensional emotion output signal is obtained from the multimodal input signal, which has the stronger emotional expression ability. Combined with the D-S evidence theory, the weighted summation method is used to fuse the multimodal information. The weighted values of the multimodal input signals corresponding to the three emotional signals are different so that more accurate and bionic emotional results can be obtained. The flowchart of the PAD three-dimensional emotion generation system is shown in Fig. 2.

The system can be described by the following formula:

$$E_{i1} = f_i(V_{text}) w_{i1} \tag{3}$$

$$E_{i2} = f_i(V_{speech}) w_{i2} \tag{4}$$

$$E_{i3} = f_i(V_{visual}) w_{i3} \tag{5}$$

$$E_i = \sum_{j=1}^{3} E_{ij}, (i = 1, 2, 3) \tag{6}$$

$$V_P = g_1(E_1) \tag{7}$$

$$V_A = g_2(E_2) \tag{8}$$

$$V_D = g_3(E_3) \tag{9}$$

where V_{text}, V_{speech}, and V_{visual} represent the voltages of input text, speech, and visual signals, respectively, w_{ij} represents the weight values for the fusion of multimodal features, which are obtained from the calculated fusion probability using the D-S synthesis rule.

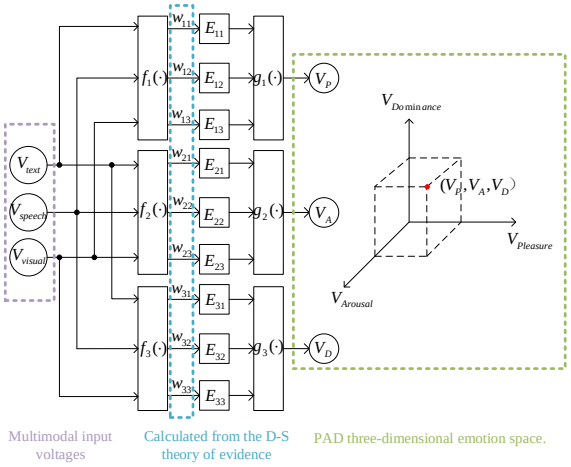

Fig. 2 Flowchart of the PAD three-dimensional emotion generation system. The multimodal input signals include text signal V_{text}, speech signal V_{speech}, and visual signal V_{visual}. The multimodal input voltages are processed by the $f_i(\cdot)$ function, multiplied by the respective weight w_{ij}, and then summed to obtain the multimodal emotional learning signal E_{ij}. After passing through the $g_i(\cdot)$ function, E_{ij} yields the emotional signal voltages, including V_P, V_A, and V_D. The weights w_{ij} are calculated using the D-S evidence theory, and (V_P,V_A,V_D) correspond to a specific emotion in the PAD three-dimensional emotional space.

$f_i(\cdot)$ is a function that satisfies the working mechanism of emotional learning in the limbic system of the brain. E_{ij} represents the single modal emotion learning signal, that is, the result of the single modal input signal after passing through the brain-like system and then multiplying with the weight. E_i represents a multimodal emotional learning signal. $g_i(\cdot)$ is a function that satisfies the working mechanism of emotion generation. V_P, V_A, and V_D represent the final output emotional signals, including the pleasure signal, arousal signal and dominance signal. The $f_i(\cdot)$ and $g_i(\cdot)$ functions corresponding to each dimension of the emotional signal are different, which is more in line with the emotional learning and generation process of the brain. The three-dimensional coordinate system consists of $V_{pleasure}$, $V_{arousal}$ and $V_{dominance}$, and (V_P,V_A,V_D) representing the final PAD three-dimensional emotional signal result.

3 Memristor model

As a two terminal ionic device that uses resistance states to represent information, memristor has rich switching dynamics, which is very suitable for simulating biological synapses and neurons.

3.1 Volatile Memristor Model

The volatile memristors (VM) [54] have a forgetting effect in which the memristance changes when voltage is applied, and the memristance automatically returns to its original state when the applied voltage disappears. In this work, VM model in (10)-(14) is used to simulate neurons from an active state to a resting state, while also ensuring that the circuit can only operate normally when a voltage is applied.

$$i = (1-x)\alpha(1-e^{-\beta v}) + x\gamma sinh(\delta v); \tag{10}$$

$$\dot{x} = (\lambda[e^{\eta_1 v} - e^{-\eta_2 v}] - \frac{x-\varepsilon}{\tau}) f(x); \tag{11}$$

$$\dot{\varepsilon} = \sigma(e^{\eta_1 v} - e^{-\eta_2 v}) f(x); \tag{12}$$

$$\dot{\tau} = \theta(e^{\eta_1 v} - e^{-\eta_2 v}); \tag{13}$$

$$f(x) = \frac{(sign(v)+1)(sign(1-x)+1) + (sign(-v)+1)(sign(x)+1)}{4}; \tag{14}$$

where i is the current and v is the applied voltage of VM; x denotes the Ohmic-like conducting channel which is normalized to be [0,1], $x = 0$ indicates fully Schottky-dominated conduction while $x = 1$ indicates fully tunneling-dominated conduction, and it is equivalent to conductance actually; α is the barrier height for Schottky barrier; β is the depletion width in the Schottky barrier region; γ is the barrier height for tunneling; δ is the effective tunneling distance in the conducting region; η_1 and η_2 are the interface effect with positive voltage and negative voltage, they are all positive-valued fitting parameters determined by material properties and dependent on x; ε is the retention of the Ohmic-like conducting channel, which is in [0,1]; λ is a positive constant to control the change rate of x; τ is the diffusion time; σ and θ are the corresponding parameters for ε and τ , which are determined by the material; $f(x)$ is the window function for better elaborating the memristor dynamics. The parameters of VM model

Table 1 THE PARAMETERS OF VM MODEL

Parameters of VM	α	β	γ	δ	η_1
Settings	0.5e-6	0.5	1e-3	1	8
Parameters of VM	η_2	λ	σ	θ	
Settings	8	0.006	0.04	0.03	

used in this work are listed in Table 1. The initial memristance of *VM* is R_{OFF} (the highest memristance). As shown in Fig. 3, if the applied voltage is positive, memristance of *VM* will decrease; after the applied voltage disappears, memristance of *VM* will increase automatically. Here a small voltage of 0.05 V is used to read the memristance currently when there is no applied voltage. In order to better test the characteristics of *VM*, *VM* is connected in series with a 1 kΩ resistor in the simulation. Fig. 3(a) shows the change in the memristance of the *VM* when the applied voltage is 1 V, and Fig. 3(b) shows the change in the memristance of the *VM* when the applied voltage is 0.6 V. Since the voltage obtained by the *VM* is proportional to the applied voltage, it is observed that the greater the applied voltage, the faster the rate of change in the memristance, and the faster it approaches R_{ON} (minimum memristance) within the same time, the longer it takes to recover to the initial memristance. Therefore different applied voltages cause changes in *VM*.

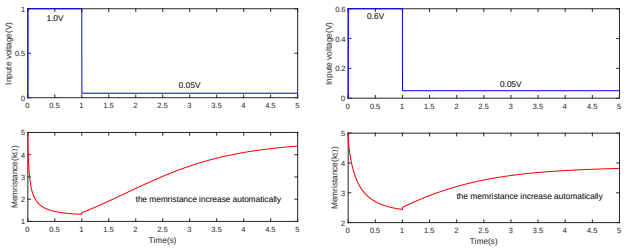

(a) (b)

Fig. 3 Memristances change of *VM* model in different applied voltages. A voltage of 1.0 V and 0.6 V is applied at 0-1.0 s, respectively, the memristance of *VM* gradually decreases from the high resistance. Between 1.0-5.0 s, there is no applied voltage in addition to a small read voltage, it can be seen that the memristance of *VM* automatically increases. The small voltage of 0.05 V is used to read the memristance currently.

3.2 Nonvolatile Memristor Model

Nonvolatile memristors are particularly suitable for the realization of neuromorphic systems due to the great plasticity in memristance. The non-volatile memristance can be reduced (increased) during the application of the potentiation (depression) voltage. In this work, the characteristics of the synaptic model of memristor are used to realize the learning and generation functions of emotions. A drift speed adaptive memristor (*DSAM*) model [55] that matches the conductive property of AgInSbTe memristor is used in this work. If the applied voltage exceeds the threshold, the memristance of the device will change, else it remains unchanged. The expression for the *DSAM* model is described as:

$$\frac{dx(t)}{dt} = \begin{cases} k_{on} v(t) \cdot f(x), & v(t) > v_{on} > 0; \\ 0\ , & v_{off} \le v(t) \le v_{on}; \\ k_{off} \cdot v(t) \cdot f(x), & v(t) < v_{off} < 0, \end{cases} \tag{15}$$

$$f(x) = \begin{cases} (a \cdot (1-x))^p, & v(t) > 0; \\ (a \cdot x)^p, & v(t) < 0, \end{cases} \tag{16}$$

$$v(t) = [R_{on} x + R_{off}(1-x)] \cdot i(t) \tag{17}$$

where state variable x is a normalized width of the conducting layer, whose derivative is matched to memristor current-voltage data. $f(x)$ is a speed adaptive state variable function. v_{on}, v_{off} are positive and negative threshold voltages respectively. k_{on}, k_{off} represent the average ion mobility of oxygen vacancies. a, p are scaling parameters, which determine the indirect effect drift speed. k_{on}, k_{off}, a and p are fitting parameters that can be adjusted to describe different memristive devices. R_{on} and R_{off} are the bounds of device resistance, whose corresponding state variable is $x(t) = 1$ and $x(t) = 0$. The change of state variable occurs only when the threshold voltage is surpassed.

Table 2 THE PARAMETERS OF *DSAM* MODEL

Parameters of *DSAM*	Setting 1	Setting 2
a	2.1	2.1
p	1.8	1.8
k_{on}	50	20
k_{off}	30	10
v_{on}(V)	0.3	0.5
v_{off}(V)	-0.3	-0.5
R_{on}(kΩ)	1	1
R_{off}(kΩ)	10	10

The parameters of *DSAM* model used in this work are listed in Table 2. As shown in Fig. 4, different parameters will lead to different memristance change rates. If the applied voltage is higher than the positive threshold voltage, the memristances of *DSAM* will decrease. If the applied voltage is lower than the negative threshold voltage, the memristances of *DSAM* will increase. In other cases, the memristances of *DSAM* remain unchanged. The initial memristance and minimum memristance of *DSAM* are set according to the actual situation, which will be described in the following work.

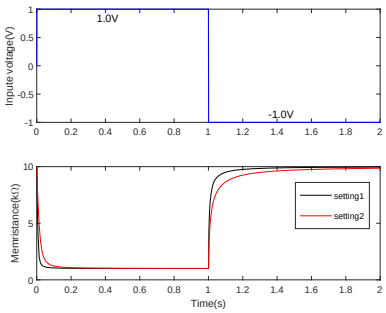

Fig. 4 Memristances change of *DSAM* memristors in two kinds of parameter settings. The black line represents the change of memristance in setting 1, and the red line represents the change of memristance in setting 2. If the applied voltage is higher than the positive threshold voltage, the memristances of *DSAM* will decrease. If the applied voltage is lower than the negative threshold voltage, the memristances of *DSAM* will increase.

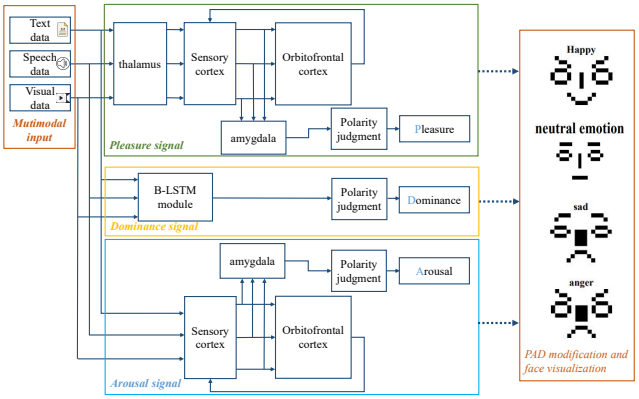

Fig. 5 The overall framework of the PAD three-dimensional emotion generation memristive circuit. The multimodal input includes text mode, speech mode and visual mode. The BEL model, B-LSTM model, D-S evidence theory and polarity judgment module are used to generate pleasure signal, arousal signal and dominance signal. The results correspond to the emotions in the three-dimensional PAD emotional space, and finally the visual face map is obtained.

4 Memristive circuit design of PAD three-dimensional emotion generation

4.1 The overall framework of emotion generation circuit

Brain tissue structures such as thalamus, sensory cortex, orbitofrontal cortex, and amygdala in the limbic system affect and produce biological emotions [5]. In order to design a bionic brain emotion generation system, this work uses the brain emotion learning model (BEL) [7] and the biological long short-term memory model (B-LSTM) [56,57]. The BEL model can simulate the interaction between organs related to emotional response, and establish a rapid emotional response mechanism for external stimuli based on the short reflex pathway of the brain. The B-LSTM model is constructed based on two types of synaptic plasticity inspired by brain memory. In this work, the volatile memristor model is used to achieve short-term plasticity, while the non-volatile memristor model is used to achieve long-term plasticity. The B-LSTM model can selectively remember long-term information without paying a great price, and is suitable for dimensional sentiment analysis.

Based on the basic models mentioned above, this work designs a complete PAD three-dimensional emotion generation memristive circuit. As shown in Fig. 5, the sensor obtains text, speech, and visual data, which are then processed by emotion algorithms to extract multimodal input signals. The multimodal input signals are modeled using the BEL model, which includes the thalamus module, the sensory cortex module, the orbitofrontal cortex module, to obtain the output of the pleasure dimension in the emotion signal. Similarly, to obtain the arousal dimension output, the multimodal input signals are modeled using the BEL model, but without the thalamus module, allowing for faster generation of arousal signals and increased sensitivity to external inputs [50]. Meanwhile, the multimodal input signals are modeled using a B-LSTM model including a short-time memory module and a long-time memory module to obtain the dominance signal. Importantly, in the amygdala module, the D-S evidence theory is used to weight the previous signals to obtain more accurate emotional signal results. In addition, the obtained pleasure signal, arousal signal, and dominance signal are numerical results of the emotion signal, while polarity requires separate determination. Therefore, the polarity judgment module are added to handle the determination of polarity. Therefore, the overall framework of this work is: First, the sensors acquire text, speech and visual data, which are then processed by software algorithms to obtain the corresponding input signals. Next, brain-like emotion generation circuits are utilized to obtain the outputs of the three dimensional emotion space, which expresses a variety of emotions. Finally, the obtained three dimensional emotion signals are processed and visualized for output.

4.2 Memristive circuit design

This work proposes a PAD three-dimensional emotion generation system based on D-S evidence theory and designs a brain-like emotion generation memristive circuit. It includes the multimodal input module, three emotional signals (pleasure signal, arousal signal, dominance signal) generation module and facial emotion visualization module. Next, it will be introduced in three

parts. The first part is multimodal input, the second part is weighted summation to generate emotional signals, and the third part is PAD emotional space representation and visual output.

4.2.1 Multimodal input

The text, speech, and visual sensors collect environmental data, and the corresponding emotional numerical scoring results are obtained by the emotion recognition algorithm respectively. The results are sent to the signal generator to obtain the pulse signal with the peak value of the emotional value, which is the multimodal input signal of the circuit. The range of emotional scoring results is [0, 1]. The closer to the maximum value, the more positive the emotion is. On the contrary, the closer to the minimum value, the more negative the emotion is. The frequency of the pulse signal generated by the signal generator is set to 20 Hz. Brain waves are some spectral bands with a strong correlation between activity and mental and emotional states in EEG [53], which can be divided into five categories. The frequency of β wave is about 13 Hz to 30 Hz, and the human state is thinking and conscious. β wave is the most common wave band in waking, which is very important in conscious states such as cognitive reasoning, calculation, reading, communication, and thinking. Higher levels of β waves have been found to have a stimulating and awakening effect, leading to anxiety, an inability to relax, elevated levels of adrenaline, and increased stress. Lower levels of β waves can result in depression, poor cognitive abilities, and lack of concentration. On the other hand, an optimal range of β waves is associated with consistent attention, strong memory, and high problem-solving abilities. Therefore, in this work, the circuit is designed with a multimodal input signal frequency of 20Hz, which better aligns with the normal wakeful state of humans.

4.2.2 Weighted summation generates emotional signals

In this work, the BEL model is used to obtain the pleasure signal, and the polarity is consistent with the polarity of the text signal. The BEL model without the thalamus module is used to obtain the arousal signal, and the polarity is consistent with the polarity of the speech signal. The B-LSTM model is used to obtain the dominant signal, which is consistent with the polarity of the visual signal.

As shown in Fig. 6, the range of multimodal input signals of text, speech, and visual is [0V, 1V]. The multimodal input signals undergo a series of processing stages, including the thalamus module, sensory cortex module, orbitofrontal cortex module and amygdala module. In the amygdala module, the signals are subjected to weighted operations, resulting in numerical values for pleasure signals. These weights are calculated using the D-S evidence theory. The signals are then further processed in the pleasure signal generation module through summation operations. Subsequently, they pass through the polarity judgment module to align the pleasure signal with the polarity of the text signal, ultimately producing the pleasure signal result. The output of this process is utilized for visualizing subsequent facial expressions. The range of the pleasure signal is [-1V, 1V]. BEL model and D-S evidence theory can simulate the information processing structure with emotional function in the brain's limbic system, and complete the emotional generation process more bionically.

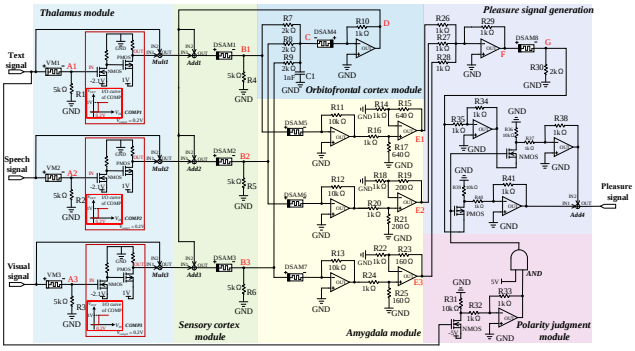

Fig. 6 Pleasure signal generating circuit. This circuit utilizes non-volatile memristors and volatile memristors to simulate synapses and neurons, respectively. It is modeled using the BEL model, replicating certain brain tissue structures within the limbic system, such as the thalamus module, sensory cortex module, orbitofrontal cortex module, and amygdala module. The amygdala module performs weighted operations with the weights calculated using the D-S evidence theory. The pleasure signal generation module performs summation operations to obtain absolute value results of the pleasure signal, and the resulting signal is then passed through the polarity judgment module to ensure that the pleasure signal is consistent with the polarity of the text signal, ultimately outputting the pleasure signal result.

In the thalamus module, the multimodal input signals pass through volatile memristors VM1-VM3 respectively, causing a decrease in their memristances and an increase in the voltages across *A1-A3*. When the voltages reach the threshold voltages of COMP1-COMP3 at 0.2V, the outputs are 1V, otherwise, the outputs are 0V. That is to say, only when the memristances of VM1-VM3 decrease to a certain value and V_{A1}-V_{A3} are greater than the threshold voltage, do the thalamus module have outputs. The signals then pass through the multipliers *Mult1-Mult3* to ensure that there are outputs when there are inputs. In the sensory cortex

module, the pulse signals output from the thalamus module are passed through the non-volatile memristors DSAM1-DSAM3 (parameters are Setting 1 in Table 2, R_{init}=9.9 kΩ, R_{on}=1 kΩ), and the input pulse signals are further processed by changing the memristances. *R4-R6* convert the current signals into the voltage signals. The orbitofrontal cortex module is used to regulate the input signals of the sensory cortex. *R7-R9* and *C1* achieve the mean value operation, namely $V_C = (V_{B1} + V_{B2} + V_{B3})/3$. DSAM4 (parameters are Setting 1 in Table 2, R_{init}=3.1 kΩ, R_{off}=10 kΩ) is connected inversely, and then through an inverse amplifier, following $V_D = -(R10/DSAM4) * V_C$, the output results are fed back to the sensory cortex module through the adders. The amygdala module is very important in emotion generation. DSAM5-DSAM7 (parameters are Setting 1 in Table 2, R_{init}=9.9 kΩ, R_{on}=2 kΩ) simulate the function of synapses. V_{B1}-V_{B3} pass through three inverse amplifiers respectively, and then pass through the in-phase amplifier to achieve weighted operation, namely $V_{E1} = 0.64 * (-R11/DSAM5)$, $V_{E2} = 0.2 * (-R12/DSAM6)$, $V_{E3} = 0.16 * (-R13/DSAM7)$.

Table 3 THE BPA OF PLEASURE SIGNAL

	$X1$	$X2$	$X3$
$P1$	0.8	0.2	0.3
$P2$	0.1	0.5	0.3
$P3$	0.1	0.3	0.4

Using D-S evidence theory, the pleasure signal is divided into three parts, namely the hypothesis recognition framework $\theta = \{P1, P2, P3\}$. The evidence from text mode, speech mode, and visual mode are $X1$, $X2$, and $X3$ after passing through the inverse amplifiers in the amygdala module. BPA is shown in Table 3. Let $P1 \cap P2 \cap P3 = P$, calculate the normalization coefficient:

$$\begin{aligned} K &= \sum_{P \neq \phi} m_1(P1)m_2(P2)m_3(P3) \\ &= 0.8 \times 0.2 \times 0.3 + 0.1 \times 0.5 \times 0.3 + 0.1 \times 0.3 \times 0.4 \\ &= 0.075 \end{aligned} \tag{18}$$

After information fusion, the probability distributions of $P1$, $P2$, and $P3$ are:

$$\begin{aligned} (m_1 \oplus m_2 \oplus m_3)P1 &= \frac{1}{K} \sum_{P=P1} m_1(P1)m_2(P2)m_3(P3) \\ &= \frac{1}{0.075} \times 0.1 \times 0.5 \times 0.3 \\ &= 0.64 \end{aligned} \tag{19}$$

$$\begin{aligned} (m_1 \oplus m_2 \oplus m_3)P2 &= \frac{1}{K} \sum_{P=P2} m_1(P1)m_2(P2)m_3(P3) \\ &= \frac{1}{0.075} \times 0.1 \times 0.3 \times 0.4 \\ &= 0.2 \end{aligned} \tag{20}$$

$$\begin{aligned} (m_1 \oplus m_2 \oplus m_3)P3 &= \frac{1}{K} \sum_{P=P3} m_1(P1)m_2(P2)m_3(P3) \\ &= \frac{1}{0.075} \times 0.8 \times 0.2 \times 0.3 \\ &= 0.16 \end{aligned} \tag{21}$$

The polarity of the pleasure signal is consistent with the polarity of the text signal. When the text signal is greater than 0.5V, the pleasure polarity is positive; otherwise, it is negative. In the polarity judgment module, the text signal is connected to an NMOS tube with a threshold voltage of 5.5V. When the polarity of the text signal is positive, the NMOS tube is turned on, and the signal is inverted and output as a 5V voltage. The signal then passes through an AND gate, and polarity judgment module ultimately outputs a high-level signal. Conversely, when the polarity of the text signal is negative, the polarity judgment module outputs a low-level signal.

In the pleasure signal generation module, firstly, the emotional signals input by the amygdala module are summed, that is, $Vf = -(Ve1 + Ve2 + Ve3)$, and then the signal is further processed by DSAM8 (parameters are Setting 2 in Table 2, R_{init}=9.9 kΩ, R_{on}=4 kΩ) and *R30* to obtain the amplitude of the pleasure signal, and then the polarity is corrected. The NMOS and PMOS tubes are used as switches. When the input signal of the polarity judgment module is high, the NMOS tube is turned on and the PMOS tube is cut off. The emotion signal V_G is then passed through two inverters and input into the adder *Add4* at IN2, where it is added to the positive polarity pleasure signal IN2 with a value of 0V at IN1. Finally, the resulting positive polarity pleasure signal is output from the OUT port. When the input signal of the polarity judgment module is low, the NMOS tube is cut off, the PMOS tube is turned on, the IN2 port of the adder *Add4* is input 0V, and the emotional signal V_G passes through an inverter to obtain a negative pleasure signal, which is input to the IN1 port of the adder *Add4*, and finally the OUT port outputs a negative pleasure signal. In this way, the polarity adjustment of the pleasure signal is realized and the correct pleasure signal is finally obtained.

As shown in Fig. 7, the arousal signal generation circuit uses a BEL model that does not pass through the thalamus module, making the brain-like system respond

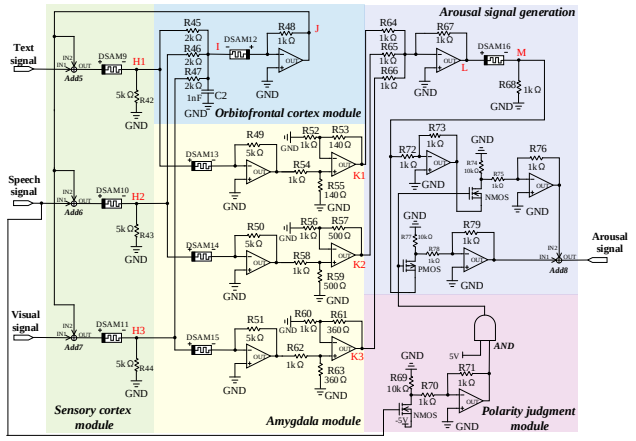

Fig. 7 Arousal signal generation circuit. This circuit is modeled using the BEL model, including the sensory cortex module, orbitofrontal cortex module, and amygdala module. The amygdala module performs weighted operations with the weights calculated using the D-S evidence theory. The arousal signal generation module performs summation operations to obtain absolute value results of the arousal signal, and the resulting signal is then passed through the polarity judgment module to ensure that the arousal signal is consistent with the polarity of the speech signal, ultimately outputting the arousal signal result.

more quickly to the stimulation of the input signal. The range of multimodal input signals of text, speech, and visual is [0V, 1V]. The multimodal input signals undergo a series of processing stages, including sensory cortex module, orbitofrontal cortex module and amygdala module. In the amygdala module, the signals are subjected to weighted operations, resulting in numerical values for arousal signals. These weights are calculated using the D-S evidence theory. The signals are then further processed in the arousal signal generation module through summation operations. Subsequently, they pass through the polarity judgment module to align the arousal signal with the polarity of the speech signal, ultimately producing the arousal signal result. The output of this process is utilized for visualizing subsequent facial expressions. The range of arousal signal is [-1V, 1V].

In the sensory cortex module, when the multimodal input signals are greater than the threshold of DSAM9-DSAM11 (parameters are Setting 1 in Table 2, R_{on}=1 kΩ), R_{init}=9.9 kΩ, the memristances decrease, the voltages at *H1-H3* points increase, and the signals are input into the orbitofrontal cortex module and amygdala module. The orbitofrontal cortex module is used to regulate the input signals of the sensory cortex, DSAM12 (parameters are Setting 1 in Table 2, R_{init}=3.1 kΩ, R_{off}=10 kΩ) is connected inversely. The amygdala module is used to further generate emotional signals. The *H1-H3* points voltage signals are respectively passed through DSAM13-DSAM15 (parameters are Setting 1 in Table 2, R_{init}=9 kΩ, R_{on}=1 k Ω) and an inverse amplifier, and then weighted by the in-phase amplifier, that is, V_{K1}=0.14*(-$R49$/ $DSAM13$), $V_{K2} = 0.5 * (-R50/DSAM14)$, $V_{K3} = 0.36 * (-R51/DSAM15)$.

Using D-S evidence theory, the arousal signal is divided into three parts, namely the hypothesis recognition framework $\theta = \{A1, A2, A3\}$. The evidence from text mode, speech mode, and visual mode are $Y1$, $Y2$, and $Y3$ after passing through the inverse amplifiers in the amygdala module. BPA is shown in Table 4. Let $A1 \cap A2 \cap A3 = A$, calculate the normalization coefficient:

Table 4 THE BPA OF AROUSAL SIGNAL

	$Y1$	$Y2$	$Y3$
$A1$	0.4	0.1	0.3
$A2$	0.3	0.7	0.2
$A3$	0.3	0.2	0.5

$$\begin{aligned} K &= \sum_{A \neq \phi} m_1(A1)m_2(A2)m_3(A3) \\ &= 0.4 \times 0.1 \times 0.3 + 0.3 \times 0.7 \times 0.2 + 0.3 \times 0.2 \times 0.5 \\ &= 0.084 \end{aligned} \tag{22}$$

After information fusion, the probability distributions of $A1$, $A2$, and $A3$ are:

$$\begin{aligned} (m_1 \oplus m_2 \oplus m_3)A1 &= \frac{1}{K} \sum_{A=A1} m_1(A1)m_2(A2)m_3(A3) \\ &= \frac{1}{0.084} \times 0.4 \times 0.1 \times 0.3 \\ &= 0.14 \end{aligned} \tag{23}$$

$$\begin{aligned} (m_1 \oplus m_2 \oplus m_3)A2 &= \frac{1}{K} \sum_{A=A2} m_1(A1)m_2(A2)m_3(A3) \\ &= \frac{1}{0.084} \times 0.3 \times 0.7 \times 0.2 \\ &= 0.5 \end{aligned} \tag{24}$$

$$\begin{aligned} (m_1 \oplus m_2 \oplus m_3)A3 &= \frac{1}{K} \sum_{A=A3} m_1(A1)m_2(A2)m_3(A3) \\ &= \frac{1}{0.084} \times 0.3 \times 0.2 \times 0.5 \\ &= 0.36 \end{aligned} \tag{25}$$

The polarity of the arousal signal is consistent with the polarity of the speech signal. When the speech signal is greater than 0.5V, the arousal polarity is positive;

otherwise, it is negative. In the arousal signal generation circuit, the output signals of the amygdala module are summed, namely, $V_L = -(V_{K1} + V_{K2} + V_{K3})$, and then the signal is further processed by DSAM16 (parameters are setting 2 in Table 2, R_{init}=9 kΩ, R_{on}=2 kΩ) and *R68*, the amplitude of the pleasure signal is $V_M = R68 * V_L/(R68 + DSAM16)$. The polarity judgment process of the arousal signal is similar to the pleasure signal and is finally output by the adder *Add8*.

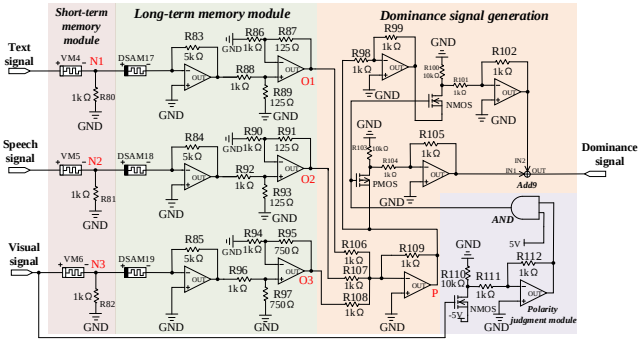

Fig. 8 Dominance signal generation circuit. The B-LSTM model is used to simulate biological short-term memory and long-term memory. The long-term memory module performs weighted operations and the weights calculated using the D-S evidence theory. The dominance signal generation module performs summation operations to obtain absolute value results of the dominance signal, and the resulting signal is then passed through the polarity judgment module to ensure that the dominance signal is consistent with the polarity of the visual signal, ultimately outputting the dominance signal result.

As shown in Fig. 8, the range of multimodal input signals of text, speech, and visual is [0V, 1V]. VM4-VM6 and *R80-R82* are used to simulate short-term memory function. When there are inputs, the memristances of the volatile memristors decrease, and the *N1-N3* point voltages increase. When there are no inputs, the memristances of VM4-VM6 automatically return to their original state. Then the signals are input into the long-term memory module and the memristances of DSAM17-DSAM19 (parameters are Setting 1 of table 2, R_{init}=8 kΩ, R_{on}=2 kΩ) change. When there are no input signals, the memristance will not return to the original state, that is, the long-term memory function is simulated. Similar to the previous amygdala module, the in-phase amplifier is used to realize the weighting function. That is $V_{O1} = 0.125 * (-R83/DSAM17)$, $V_{O2} = 0.125 * (-R84/DSAM18)$, $V_{O3} = 0.75 * (-R97/DSAM19)$.

Using D-S evidence theory, the dominance signal is divided into three parts, namely the hypothesis recognition framework $\theta = \{D1, D2, D3\}$. The evidence from text mode, speech mode, and visual mode are $Y1$, $Y2$, and $Y3$ after passing through the inverse amplifiers in the amygdala module. BPA is shown in Table 5. Let $D1 \cap D2 \cap D3 = D$, calculate the normalization coefficient:

Table 5 THE BPA OF DOMINANCE SIGNAL

	$Z1$	$Z2$	$Z3$
$D1$	0.4	0.3	0.1
$D2$	0.3	0.4	0.1
$D3$	0.3	0.3	0.8

$$\begin{aligned} K &= \sum_{D \neq \phi} m_1(D1)m_2(D2)m_3(D3) \\ &= 0.4 \times 0.3 \times 0.1 + 0.3 \times 0.4 \times 0.1 + 0.3 \times 0.3 \times 0.8 \\ &= 0.096 \end{aligned} \tag{26}$$

After information fusion, the probability distributions of $D1$, $D2$, and $D3$ are:

$$\begin{aligned} (m_1 \oplus m_2 \oplus m_3)D1 &= \frac{1}{K} \sum_{D=D1} m_1(D1)m_2(D2)m_3(D3) \\ &= \frac{1}{0.096} \times 0.4 \times 0.3 \times 0.1 \\ &= 0.125 \end{aligned} \tag{27}$$

$$\begin{aligned} (m_1 \oplus m_2 \oplus m_3)D2 &= \frac{1}{K} \sum_{D=D2} m_1(D1)m_2(D2)m_3(D3) \\ &= \frac{1}{0.096} \times 0.3 \times 0.4 \times 0.1 \\ &= 0.125 \end{aligned} \tag{28}$$

$$\begin{aligned} (m_1 \oplus m_2 \oplus m_3)D3 &= \frac{1}{K} \sum_{D=D3} m_1(D1)m_2(D2)m_3(D3) \\ &= \frac{1}{0.096} \times 0.3 \times 0.3 \times 0.8 \\ &= 0.75 \end{aligned} \tag{29}$$

The polarity of the dominance signal is consistent with the polarity of the visual signal. When the visual signal is greater than 0.5V, the dominance polarity is positive; otherwise, it is negative. In the dominance signal generation circuit, the output signals of the long-term memory module are summed, that is, the value of the pleasure signal is $V_P = -(V_{O1} + V_{O2} + V_{O3})$. The principle of the polarity judgment module is the same as the previous emotional signal so that the polarity of the dominance signal is consistent with the polarity of the visual signal, and the final result is output through the adder *Add9*. The range of the dominant signal is [-1V, 1V].

4.2.3 PAD emotional space representation and visualization

Based on the above basic theory and circuit design, the multimodal input signals of text, speech, and visual generate the emotional signals of the PAD emotional model, that is, the pleasure signal, the arousal signal, and the dominance signal. The range of the signal is [-1V, 1V]. The three signals form the final emotion in the PAD three-dimensional space, and the coordinate origin (0V, 0V, 0V) in the space is neutral emotion.

To represent emotions more intuitively and specifically, this work inputs the final output of the circuit's pleasure signal, arousal signal, and dominance signal results into MATLAB to realize facial emotion visualization. The neutral emotional face is shown in Fig. 9.

Fig. 9 Natural face image. The output of the PAD model is (0V, 0V, 0V) corresponding to the neutral emotional face image.

Using eyebrows, eyes, nose, and mouth to express emotions. The pleasure signal represents the degree of psychological pleasure. When the pleasure signal polarity is positive, the nose appears thinner. When the pleasure signal polarity is negative, the nose is wider. The polarity of the arousal signal represents the level of psychological alertness. When the polarity of the pleasure signal is positive, the eyes are larger, and when the polarity is negative, the eyes are smaller. The dominance signal represents the degree of subjective control of the emotional state and affects the curved shape of eyebrows and mouths. The specific visual face image will be explained in detail in the next section.

5 Circuit simulation and analysis of memristive PAD three-dimensional emotion generation

5.1 Simulation results

The text signal, speech signal, and visual signal are pulse signals with a frequency of 20Hz, where the amplitude represents the intensity of emotions. The signal range is [0V, 1V]. When the signal is greater than 0.5V, the polarity is considered positive, otherwise, it is negative. Text, speech, and visual signals can have eight polarity combinations, namely eight input modes, as shown in Table 6. '+' means the polarity of the input signal is positive, and '-' means the polarity of the input signal is negative. Each mode is simulated in PSPICE to verify the feasibility of the circuit.

Table 6 THE AMPLITUDE OF INPUT SIGNALS

Input mode	Text signal	Speech signal	Visual signal
1	0.95(+)	0.75(+)	0.51(+)
2	0.75(+)	0.30(-)	0.99(+)
3	0.78(+)	0.85(+)	0.15(-)
4	0.38(-)	0.79(+)	0.95(+)
5	0.80(+)	0.15(-)	0.10(-)
6	0.40(-)	0.80(+)	0.40(-)
7	0.30(-)	0.45(-)	0.86(+)
8	0.22(-)	0.28(-)	0.35(-)

Using the first input mode from Table 6 as an example, we observe the change in memristance of the eight non-volatile memristors to simulate the process of brain-like emotion generation. Through this simulation, we can obtain the pleasure signal, arousal signal, and dominance signal. Fig.10 shows the pulse waveform of the signals in the first input mode, and the results of the three emotional signals: pleasure signal, arousal signal and dominance signal.

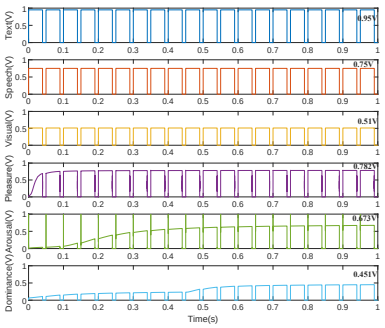

Fig. 10 The first input mode. The amplitudes of the text, speech and visual pulse signals are 0.95V, 0.75V and 0.51V, respectively. The final pleasure signal, arousal signal and dominance signal are 0.782V, 0.673V and 0.451V, respectively.

The memristance changes of non-volatile memristors DSAM1-DSAM8 in the pleasure signal generation module is shown in Fig.11. The input signals pass through the thalamus module to obtain the outputs of *mult1-mult3*. The larger the amplitude of the input pulse signals, the larger the output signals. In the sensory cortex module, the output signals exceed the threshold of DSAM1-DSAM3, resulting in the decrease of their memristances, and the results of V_{B1}-V_{B3} change accordingly. The memristance of DSAM4 in the orbitofrontal

cortex module increases to obtain the V_D that regulates the emotional signal. The orbitofrontal cortex module feeds back the V_D signal to the sensory cortex module to indirectly regulate the emotional signal. The V_{B1}-V_{B3} signals pass through the amygdala module, which reduces the memristances of DSAM5-DSAM7, and is weighted by the proportional circuit to obtain V_{E1}-V_{E3}. They are then summed by pleasure signal generation module, so that the memristance of DSAM8 is reduced, and the pleasure signal amplitude result V_G is obtained. The polarity judgment module judges pleasure signal as positive, and finally outputs the the pleasure signal $V_{pleasure}$.

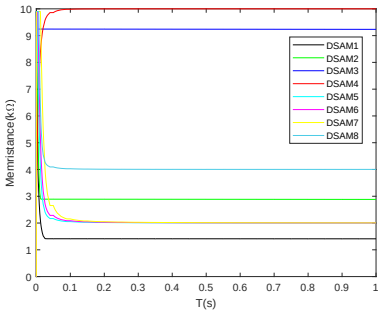

Fig. 11 In the first input mode, the memristance change of non-volatile memristors DSAM1-DSAM8 in the pleasure signal generation module.

The memristance changes of the non-volatile memristors DSAM9-DSAM16 in the arousal signal generation module is shown in Fig. 12. In the sensory cortex module, the input signals exceed the threshold of DSAM9-DSAM11, resulting in the decrease of their memristances, and the results of V_{H1}-V_{H3} change accordingly. In the orbitofrontal cortex module, the memristance of DSAM12 increases to obtain the V_J that regulates the emotional signal. The orbitofrontal cortex module feeds back the V_J signal to the sensory cortex module to indirectly regulate the regulation of emotional signals. The V_{H1}-V_{H3} signals pass through the amygdala module, which reduces the memristances of DSAM13-DSAM15, and is weighted by the proportional circuit to obtain V_{K1}-V_{K3}. They are then summed by the arousal signal generation module, so that the memristance of DSAM16 is reduced, and the amplitude result V_M of arousal signal is obtained. The polarity judgment module judges the arousal signal as positive, and finally outputs the arousal signal $V_{arousal}$.

The memristance changes of non-volatile memristor DSAM17-DSAM19 in the dominance signal generation module is shown in Fig. 13. The input signals pass through the short-term memory module to obtain V_{N1}-V_{N3}. In the long-term memory module, V_{N1}-V_{N3}

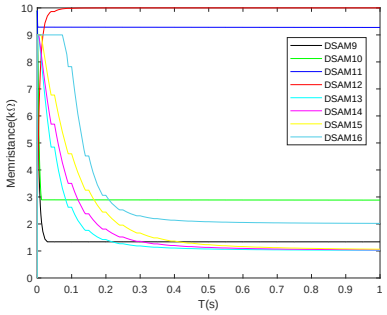

Fig. 12 In the first input mode, the memristance change of non-volatile memristors DSAM9-DSAM16 in the arousal signal generation module.

are greater than the threshold of DSAM17-DSAM19, resulting in a decrease in their memristances. Then the signals are weighted by the proportional circuit to obtain V_{O1}-V_{O3}. They are then summed by the dominance signal generation module, and combine the results of the polarity judgment module to finally output the positive dominance signal $V_{dominance}$.

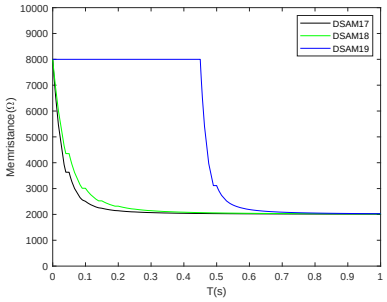

Fig. 13 In the first input mode, the memristance change of non-volatile memristors DSAM17-DSAM19 in the dominance signal generation module.

The simulation results of other input modes in Table 6 are shown in Fig. 14- 20. It can be found that the eight input signal polarity combinations can obtain emotional results scattered in eight quadrants in three-dimensional space. Eight emotional results are shown in Table 7. PAD three-dimensional emotional space results are shown in Fig. 21.

Table 7 EMOTIONAL RESULTS OF SIMULATION EXPERIMENTS UNDER EIGHT INPUT MODES

$V_{pleasure}$(V)	$V_{arousal}$(V)	$V_{dominance}$(V)	emotion
0.782	0.673	0.451	Happy
0.655	-0.654	0.844	Relaxed
0.595	0.524	-0.197	Dependent
-0.503	0.781	0.797	Anger
0.470	-0.035	-0.103	Meek
-0.17	0.389	-0.146	Fear
-0.136	-0.306	0.601	Contemptuous
-0.01	-0.03	-0.058	Sad

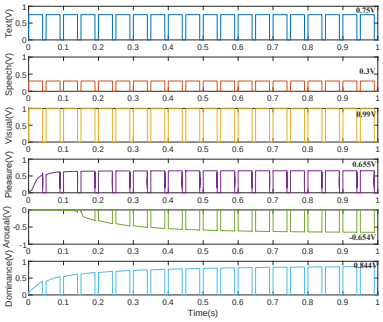

Fig. 14 In the second input mode in Table 6, the waveform of input signals and emotional signals in the brain-like emotion generation memristive circuit. The amplitudes of the text, speech and visual pulse signals are 0.75V, 0.3V and 0.99V, respectively. The final pleasure signal, arousal signal and dominance signal are 0.655V, -0.654V and 0.844V, respectively.

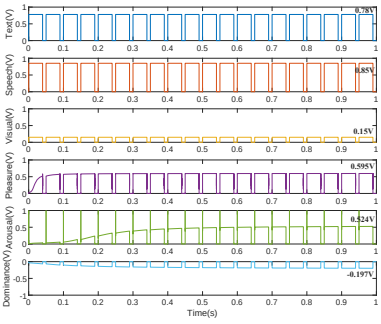

Fig. 15 In the third input mode in Table 6, the waveform of input signals and emotional signals in the brain-like emotion generation memristive circuit. The amplitudes of the text, speech and visual pulse signals are 0.78V, 0.85V and 0.15V, respectively. The final pleasure signal, arousal signal and dominance signal are 0.595V, 0.524V and -0.197V, respectively.

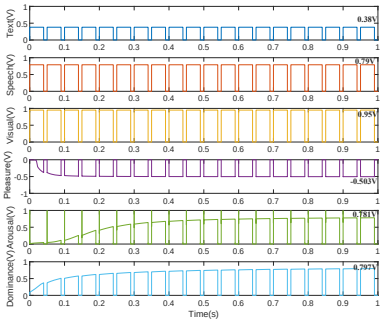

Fig. 16 In the fourth input mode in Table 6, the waveform of input signals and emotional signals in the brain-like emotion generation memristive circuit. The amplitudes of the text, speech and visual pulse signals are 0.38V, 0.79V and 0.95V, respectively. The final pleasure signal, arousal signal and dominance signal are -0.503V, 0.781V and 0.797V, respectively.

On the positive polarity of each dimension of the PAD three-dimensional emotion model, the neutral emotion value is 0V, and the maximum value is 1V. Taking the pleasure signal as an example, the value of the

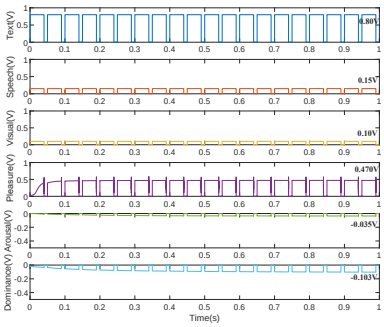

Fig. 17 In the fifth input mode in Table 6, the waveform of input signals and emotional signals in the brain-like emotion generation memristive circuit. The amplitudes of the text, speech and visual pulse signals are 0.80V, 0.15V and 0.10V, respectively. The final pleasure signal, arousal signal and dominance signal are 0.470V, -0.035V and -0.103V, respectively.

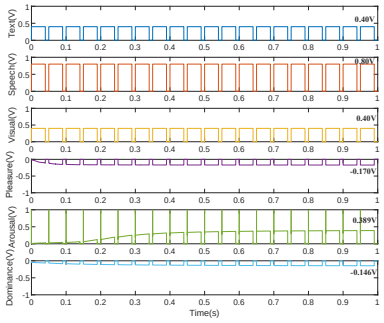

Fig. 18 In the sixth input mode in Table 6, the waveform of input signals and emotional signals in the brain-like emotion generation memristive circuit. The amplitudes of the text, speech and visual pulse signals are 0.40V, 0.80V and 0.40V, respectively. The final pleasure signal, arousal signal and dominance signal are -0.170V, 0.389V and -0.146V, respectively.

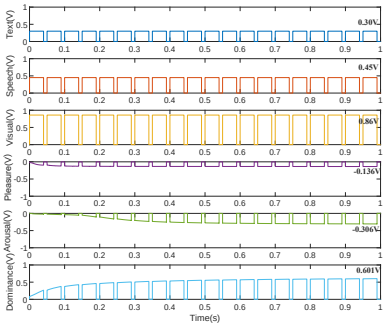

Fig. 19 In the seventh input mode in Table 6, the waveform of input signals and emotional signals in the brain-like emotion generation memristive circuit. The amplitudes of the text, speech and visual pulse signals are 0.30V, 0.45V and 0.86V, respectively. The final pleasure signal, arousal signal and dominance signal are -0.136V, -0.306V and 0.601V, respectively.

emotional signal is from 0V to 1V, indicating that the emotion is more excited. In the negative polarity of each dimension, the minimum value is -1V and the maximum

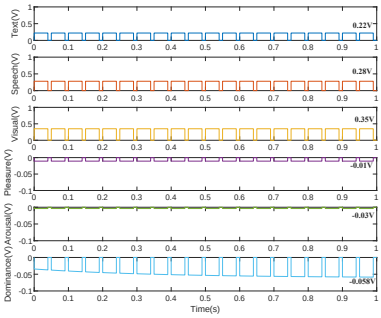

Fig. 20 In the eighth input mode in Table 6, the waveform of input signals and emotional signals in the brain-like emotion generation memristive circuit. The amplitudes of the text, speech and visual pulse signals are 0.22V, 0.28V and 0.35V, respectively. The final pleasure signal, arousal signal and dominance signal are -0.01V, -0.03V and -0.058V, respectively.

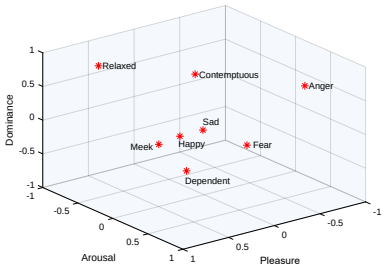

Fig. 21 PAD three-dimensional emotional space results under eight input modes. Eight emotions in three-dimensional space are distributed in eight quadrants.

value is 0V. Taking the pleasure signal as an example, when the value of the emotional signal is from -1V to 0V (not included), it means that the emotion is sadder and sadder. It can be seen that through the proposed circuit, different input signals can produce different emotions in different environments.

Finally, according to the experimental results of the emotional signals, the data are imported into MATLAB for simulation, and the corresponding face images are obtained to realize the visual outputs, as shown in Fig. 22.

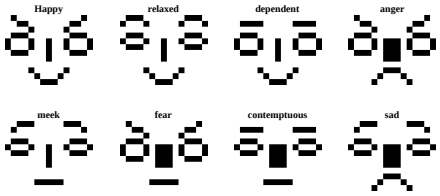

Fig. 22 The corresponding emotional visualization output face images under the eight input modes in Table 6.

5.2 Analysis

By analyzing the input signals in Table 6 and the simulation results in Table 7, it can be observed that the proposed PAD three-dimensional emotion generation memristive system is able to generate different emotions like human beings, and there exists a nonlinear mapping relationship between circuit inputs and outputs. This proves that the proposed circuit has bionic brain-like emotion generation ability, and the emotional results are more accurate and the emotional expression range is larger. Figure 23 draws the complete experimental flowchart of this work. The sensors acquire multimodal data, and then the signal generators produce pulse signals, and the pulse signals are input into the proposed brain-like bionic circuit to obtain the emotion signals. In this work, the pleasure signal is considered to have the same polarity as the text signal, the arousal signal is considered to have the same polarity as the speech signal, the dominance signal is considered to have the same polarity as the visual signal. The emotion signals pass through the polarity judgment module to get the final output signals. Taking the first mode as an example, the input pulse signal amplitudes are (0.95V, 0.75V, 0.51V), and the generated emotion signal results are (0.782V, 0.673V, 0.451V). Since all the input signal amplitudes are greater than 0.5V, the output signals have positive polarity, resulting in the final output signals of (0.782V, 0.673V, 0.451V). This indicatesa positive, highly active, subjective emotion, i.e., the emotion "happy". The facial expression associated with "happy" includes raised eyebrows, widened eyes, narrowed nostrils, and upward-turned corners of the mouth. Further analysis of the other seven simulation results leads to the following conclusions:

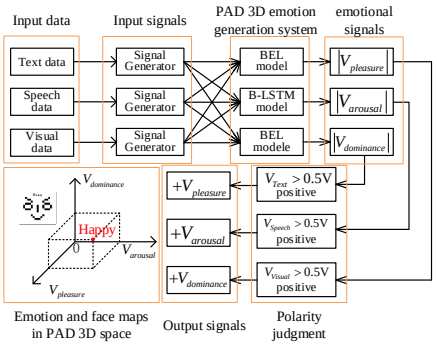

Fig. 23 Flowchart of the complete experiment based on the proposed system.

1. The multimodal input signals are pulse signals. The amplitude of the text signal, speech signal and visual

signal affects the amplitude of the pleasure signal, arousal signal and dominance signal. The weights of multimodal input signals corresponding to three-dimensional emotional signals are different. In this work, the BEL model, B-LSTM model and D-S evidence theory are used to obtain more bionic and more accurate emotional signal amplitude results.
2. The polarity of the pleasure signal, arousal signal and dominance signal is related to the value of the text signal, speech signal and visual signal respectively. Using the PAD three-dimensional emotion model, the eight input modes of this work can be distributed in eight spaces, dividing emotions more completely and accurately.
3. According to the amplitude and polarity of the pleasure signal, the arousal signal and the dominance signal, eight face images can be obtained from the eight simulation results to visualize the emotions, making the results more intuitive.

Table 8 COMPARISON BETWEEN THE PROPOSED WORK WITH THE OTHER WORKS

	Implementation way	Brain-Like mechanism	Emotional expression model	Dimensional differences
[21]	software	NO	V-A(2D)	NO
[22]	software	NO	discrete	NO
[42]	analog	NO	discrete	NO
[44]	analog	NO	discrete	NO
[45]	analog	YES	discrete	NO
[48]	analog	YES	Rolls(1D)	NO
[49]	analog	YES	V-A(2D)	NO
this work	analog	YES	PAD(3D)	YES

Table 8 compares the proposed work with other studies related to emotion generation. It can be observed that this work simulates parts of biological mechanisms of brain emotion generation, using memristors to simulate synapses and neurons, constructing brain tissue structures, optimizing circuit architecture, and hardware to realize a more bionic brain-like emotion generation function. The PAD three-dimensional emotion expression model better conforms to human-like emotions, and the D-S evidence theory effectively expresses the emotional differences of the PAD model. The system utilizes the weighted summation method for feature fusion to obtain more accurate emotion results.

6 Conclusion

In this work, a PAD three-dimensional brain-like emotion generation system is proposed, and an emotion generation memristive circuit is designed according to the system. The circuit can generate emotions like human beings under the influence of text features, speech features and visual features, and express emotions in three-dimensional space, namely, pleasure dimension, arousal dimension and dominance dimension. The circuit uses memristors to simulate synapses and neurons and combines the BEL model and B-LSTM model to simulate the emotional generation mechanism and biological memory theory of the limbic system of the brain, making the circuit structure bionic and concise. The circuit is also combined with D-S evidence theory to simulate the influence of multimodal input signals on the weight of each dimensional emotional signal, which makes the circuit more bionic and emotional expression more accurate. Each dimension in the PAD three-dimensional emotion model is a measure of a certain aspect of emotion, which can effectively explain human emotions and have a wider range of emotional expressions. This work also realizes the visual expression of emotion, which is more intuitive. In addition, the system receives external features from the sensor, generates emotional signals in the circuit, and finally obtains a visual face image. It is a complete bionic simulation system that can be used in specific scenarios. For example, for people who need emotional companionship, designing emotional robots can more accurately generate emotions and interact with them. Next, we can optimize the circuit structure, consider personality factors, etc., to achieve a more bionic, better performance, and larger brain-like emotion generation system.

Funding

This work was supported by the National Natural Science Foundation of China (Nos.62271197, 61971185.)

Data Availability Statement

Data sharing is not applicable to this article, as no datasets were generated or analysed during the current study.

Declaration

Conflict of interest

The authors declare that they have no known competing financial interests or personal relationships that could have appeared to influence the work reported in this paper.

References

1. Sendhoff, B., Koerner, E., Sporns, O.: Creating brain-like intelligence. In: From basic principles to complex intelligent systems, vol. 5436, pp. 1+ (2009)
2. Roy, K., Jaiswal, A., Panda, P.: Towards spike-based machine intelligence with neuromorphic computing. Nature **575**(7784), 607–617 (2019). DOI 10.1038/s41586-019-1677-2
3. Catani, M., Dell'Acqua, F., Thiebaut de Schotten, M.: A revised limbic system model for memory, emotion and behaviour. Neurosci. Biobehav. Rev. **37**(8), 1724–1737 (2013). DOI 10.1016/j.neubiorev.2013.07.001
4. Pessoa, L.: A network model of the emotional brain. Trends Cognit. Sci. **21**(5), 357–371 (2017). DOI 10.1016/j.tics.2017.03.002
5. Lautin, A.: Maclean's limbic system. Springer US, Boston, MA (2001)
6. Tyng, C.M., Amin, H.U., Saad, M.N.M., Malik, A.S.: The influences of emotion on learning and memory. Front. Psychol. **8**, 1454 (2017). DOI 10.3389/fpsyg.2017.01454
7. Moren, J., Balkenius, C.: A computational model of emotional learning in the amygdala. In: From Animals to Animats 6, pp. 383–391 (2000)
8. Sharbafi, M.A., Lucas, C., Daneshvar, R.: Motion control of omni-directional three-wheel robots by brain-emotional-learning-based intelligent controller. IEEE Trans. Syst. Man Cybern. Part C Appl. Rev. **40**(6), 630–638 (2010). DOI 10.1109/TSMCC.2010.2049104
9. Jafarzadeh, S., Mirheidari, R., Motlagh, M.J., Barkhordari, M.: Designing pid and belbic controllers in path tracking and collision problem in automated highway systems. In: 2008 10th International Conference on Control, Automation, Robotics and Vision, pp. 1562–1566 (2008). DOI 10.1109/ICARCV.2008.4795757
10. Asad, M.U., Farooq, U., Gu, J., Amin, J.: Neo-fuzzy supported brain emotional learning based pattern recognizer for classification problems. IEEE Access **5**, 6951–6968 (2017). DOI 10.1109/ACCESS.2017.2698419
11. Xu, C., Wang, C., Jiang, J., Sun, J., Lin, H.: Memristive circuit implementation of context-dependent emotional learning network and its application in multitask. IEEE Trans. Comput. Aided Des. Integr. Circuits Syst. **41**(9), 3052–3065 (2022). DOI 10.1109/TCAD.2021.3116463
12. Lotfi, E., Akbarzadeh-T, M.R.: Brain emotional learning-based pattern recognizer. Cybern. Syst. **44**(5), 402–421 (2013). DOI 10.1080/01969722.2013.789652
13. Ying, M., Guan-Zheng, T., Zhen-Tao, L., He, W.: Chaotic time series prediction based on brain emotional learning model and self-adaptive genetic algorithm. Acta Physica Sinica **67**(8), 080502 (2018). DOI 10.7498/aps.67.20172104
14. Thendral, M.T., Babu, T.R.G., Chandrasekar, A., Cao, Y.: Synchronization of markovian jump neural networks for sampled data control systems with additive delay components: analysis of image encryption technique. Math. Methods Appl. Sci. (2022). DOI 10.1002/mma.8774
15. Chandrasekar, A., Radhika, T., Zhu, Q.: State estimation for genetic regulatory networks with two delay components by using second-order reciprocally convex approach. Neural Process. Lett. **54**(1), 327–345 (2022). DOI 10.1007/s11063-021-10633-4
16. A. Chandrasekar, T. Radhika, and Q. Zhu: Further results on input-to-state stability of stochastic cohen-grossberg bam neural networks with probabilistic time-varying delays. Neural Process. Lett. **54**(1), 613–635 (2022). DOI 10.1007/s11063-021-10649-w
17. Radhika, T., Chandrasekar, A., Vijayakumar, V., Zhu, Q.: Analysis of markovian jump stochastic cohen-grossberg bam neural networks with time delays for exponential input-to-state stability. Neural Process. Lett. **55**, 11055–11072 (2023). DOI 10.1007/s11063-023-11364-4
18. Cao, Y., Chandrasekar, A., Radhika, T., Vijayakumar, V.: Input-to-state stability of stochastic markovian jump genetic regulatory networks. Math. Comput. Simul. (2023). DOI 10.1016/j.matcom.2023.08.007
19. Chae, Y.J., Jeon, T.H., Kim, C., Park, S.K.: Text-based robot emotion and human-like emotional transition. In: 2021 IEEE/RSJ International Conference on Intelligent Robots and Systems (IROS), pp. 838–845 (2021). DOI 10.1109/IROS51168.2021.9636793
20. Li, Y., Ishi, C.T., Inoue, K., Nakamura, S., Kawahara, T.: Expressing reactive emotion based on multimodal emotion recognition for natural conversation in human-robot interaction*. Adv. Rob. **33**(20), 1030–1041 (2019). DOI 10.1080/01691864.2019.1667872
21. Churamani, N., Barros, P., Gunes, H., Wermter, S.: Affect-driven learning of robot behaviour for collaborative human-robot interactions. Front. Rob. AI **9**, 717193 (2022). DOI 10.3389/frobt.2022.717193
22. Hong, A., Lunscher, N., Hu, T., Tsuboi, Y., Zhang, X., Alves, S.F.d.R., Nejat, G., Benhabib, B.: A multimodal emotional human-robot interaction architecture for social robots engaged in bidirectional communication. IEEE Trans. Cybern. **51**(12), 5954–5968 (2021). DOI 10.1109/TCYB.2020.2974688
23. Sebastian, A., Le Gallo, M., Khaddam-Aljameh, R., Eleftheriou, E.: Memory devices and applications for in-memory computing. Nat. Nanotechnol. **15**(7), 529–544 (2020). DOI 10.1038/s41565-020-0655-z
24. He, Z., Wang, T., Meng, J., Zhu, H.: Cmos back-end compatible memristors for in situ digital and neuromorphic computing applications. Mater. Horiz. **8**(12), 3345–3355 (2021). DOI 10.1039/d1mh01257f
25. Zhou, G., Wang, Z., Sun, B., Zhou, F., Sun, L.: Volatile and nonvolatile memristive devices for neuromorphic computing. Adv. Electron. Mater. **8**(7), 2101127 (2022). DOI 10.1002/aelm.202101127
26. Sun, J., Jiang, M., Zhou, Q., Wang, C., Sun, Y.: Memristive cluster based compact high-density nonvolatile memory design and application for image storage. Micromachines **13**(6), 844 (2022). DOI 10.3390/mi13060844
27. Sun, J., Kang, K., Sun, Y., Hong, Q., Wang, C.: A multi-value 3d crossbar array nonvolatile memory based on pure memristors. Eur. Phys. J. Spec. Top. **231**(16-17, SI), 3119–3130 (2022). DOI 10.1140/epjs/s11734-022-00576-9
28. Deng, Z., Wang, C., Lin, H., Sun, Y.: A memristive spiking neural network circuit with selective supervised attention algorithm. IEEE Trans. Comput. Aided Des. Integr. Circuits Syst. **42**(8), 2604–2617 (2022). DOI 10.1109/TCAD.2022.3228896
29. Zhou, C., Sun, Y., Yao, W., Lin, H.: Cluster output synchronization for memristive neural networks. Inf. Sci. **589**, 459–477 (2021). DOI 10.1016/j.ins.2021.12.084
30. Zhou, C., Wang, C., Yao, W., Lin, H.: Observer-based synchronization of memristive neural networks under dos attacks and actuator saturation and its application to image encryption. Appl. Math. Comput. **425**, 127080 (2022). DOI 10.1016/j.amc.2022.127080
31. Liao, M., Sun, Y., Lin, H., Xu, C.: Memristor-based affective associative memory neural network circuit with emotional gradual processes. Neural Comput. Appl. **34**, 1–16 (2022). DOI 10.1007/s00521-022-07170-z

32. Hong, Q., Shi, Z., Sun, J., Du, S.: Memristive self-learning logic circuit with application to encoder and decoder. Neural Comput. Appl. **33**, 4901–4913 (2021). DOI 10.1007/s00521-020-05281-z
33. Xu, C., Sun, J., deng, Q.: A memristor-based associative memory neural network circuit with emotion effect. Neural Comput. Appl. pp. 1–16 (2023). DOI 10.1007/s00521-023-08275-9
34. Ma, M., Xiong, K., Li, Z., Sun, Y.: Dynamic behavior analysis and synchronization of memristor-coupled heterogeneous discrete neural networks. Mathematics **11**(2), 375 (2023). DOI 10.3390/math11020375
35. Rakkiyappan, R., Chandrasekar, A., Cao, J.: Passivity and passification of memristor-based recurrent neural networks with additive time-varying delays. IEEE Trans. Neural Networks Learn. Syst. **26**(9), 2043–2057 (2015). DOI 10.1109/TNNLS.2014.2365059
36. Tang, D., Wang, C., Lin, H., Yu, F.: Dynamics analysis and hardware implementation of multi-scroll hyperchaotic hidden attractors based on locally active memristive hopfield neural network. Nonlinear Dyn. **112**, 1511–1527 (2024). DOI 10.1007/s11071-023-09128-9
37. Deng, Q., Wang, C., Lin, H.: Memristive hopfield neural network dynamics with heterogeneous activation functions and its application. Chaos, Solit. Fract. **178**, 114387 (2024). DOI 10.1016/j.chaos.2023.114387
38. Wang, C., Tang, D., Lin, H., Yu, F., Sun, Y.: High-dimensional memristive neural network and its application in commercial data encryption communication. Expert Syst. Appl. **242**, 122513 (2024). DOI 10.1016/j.eswa.2023.122513
39. Lin, H., Wang, C., Yu, F., Hong, Q., Xu, C., Sun, Y.: A triple-memristor hopfield neural network with space multistructure attractors and space initial-offset behaviors. IEEE Trans. Comput. Aided Des. Integr. Circuits Syst. **42**(12), 4948–4958 (2023). DOI 10.1109/TCAD.2023.3287760
40. Wen, Z., Wang, C., Deng, Q., Lin, H.: Regulating memristive neuronal dynamical properties via excitatory or inhibitory magnetic field coupling. Nonlinear Dyn. **110**, 3823 – 3835 (2022). DOI 10.1007/s11071-022-07813-9
41. Ma, X., Wang, C., Qiu, W., Yu, F.: A fast hyperchaotic image encryption scheme. Int. J. Bifurc. Chaos **33**(5), 2350061 (2023). DOI 10.1142/S021812742350061X
42. Ma, D., Wang, G., Han, C., Shen, Y., Liang, Y.: A memristive neural network model with associative memory for modeling affections. IEEE Access **6**, 61614–61622 (2018). DOI 10.1109/ACCESS.2018.2875433
43. Wang, Z., Hong, Q., Wang, X.: Memristive circuit design of emotional generation and evolution based on skin-like sensory processor. IEEE Trans. Biomed. Circuits Syst. **13**(4), 631–644 (2019). DOI 10.1109/TBCAS.2019.2923055
44. Sun, J., Xiao, X., Liu, P., Wang, Y.: Memristive circuits design under different personality traits based on second-order damping system. Microelectron. J. **114**, 105148 (2021). DOI 10.1016/j.mejo.2021.105148
45. Zhou, H., Fei, Z., Hong, Q., Sun, J., Du, S., Li, T., Zhang, J.: Bionic dual-loop emotional learning circuit and its application in radiation early warning monitoring. IEEE Trans. Cognit. Dev. Syst. **15**(3), 1196–1208 (2023). DOI 10.1109/TCDS.2022.3200470
46. Ekman, P., Friesen, W., O'Sullivan, M.: Universals and cultural differences in the judgments of facial expressions of emotion. Journal of personality and social psychology **53**, 712–7 (1987). DOI 10.1037/0022-3514.53.4.712
47. Slama, M.: Emotions and life: Perspectives from psychology, biology, and evolution. Psychology & Marketing **22**, 97–107 (2005). DOI 10.1002/mar.20048
48. Zhang, Y., Zeng, Z.: Neuromorphic circuit implementation of operant conditioning based on emotion generation and modulation. IEEE Trans. Circuits Syst. I Regul. Pap. **70**(5), 1868–1881 (2023). DOI 10.1109/TCSI.2023.3243773
49. Wang, Z., Wang, X., Zeng, Z.: Memristive circuit design of brain-like emotional learning and generation. IEEE Trans. Cybern. **53**(1), 222–235 (2023). DOI 10.1109/TCYB.2021.3090811
50. Z. Wang, X. Wang, and Z. Zeng: Memristive circuit design of brain-inspired emotional evolution based on theories of internal regulation and external stimulation. IEEE Trans. Biomed. Circuits Syst. **15**(6), 1380–1392 (2021). DOI 10.1109/TBCAS.2021.3127573
51. Russell, J.: A circumplex model of affect. Journal of Personality and Social Psychology **39**, 1161–1178 (1980). DOI 10.1037/h0077714
52. Mehrabian, A.: Basic dimensions for a general psychological theory: Implications for personality, social, environmental, and developmental studies. Cambridge: Oelgeschlager, Gunn & Hain (1980)
53. Teplan, M.: Fundamental of eeg measurement. Measurement Science Review **2**(2), 1–11 (2002)
54. Chen, L., Li, C., Huang, T., Hu, X., Chen, Y.: The bipolar and unipolar reversible behavior on the forgetting memristor model. Neurocomputing **171**, 1637–1643 (2016). DOI 10.1016/j.neucom.2015.06.067
55. Fu, H., Hong, Q., Wang, C., Sun, J., Li, Y.: Solving non-homogeneous linear ordinary differential equations using memristor-capacitor circuit. IEEE Trans. Circuits Syst. I Regul. Pap. **68**(11), 4495–4507 (2021). DOI 10.1109/TCSI.2021.3111620
56. Bliss, T.V.P., Collingridge, G.L., Collingridge, G.L.: A synaptic model of memory: long-term potentiation in the hippocampus. Nature **361**(6407), 31–39 (1993). DOI 10.1038/361031A0
57. Whitlock, J.R., Whitlock, J.R., Heynen, A.J.: Learning induces long-term potentiation in the hippocampus. Science **313**(5790), 1093–1097 (2006). DOI 10.1126/SCIENCE.1128134